Laser and Optical System for Laser Assisted Hydrogen Ion Beam Stripping at SNS

Y. Liu, A. Rakhman, A. Menshov, A. Webster, T. Gorlov, A. Aleksandrov, S. Cousineau

Spallation Neutron Source

Oak Ridge National Laboratory

Oak Ridge, TN 37831, U.S.A.

Corresponding Author:

Yun Liu

Spallation Neutron Source

Oak Ridge National Laboratory

1 Bethel Valley Road, Oak Ridge, TN 37831 USA

Phone: (865) 241-2063

Fax: (865) 576-9209

Email: liuy2@ornl.gov

Abstract

Recently, a high-efficiency laser assisted hydrogen ion (H-) beam stripping was successfully carried out in the Spallation Neutron Source (SNS) accelerator. The experiment was not only an important step toward foil-less H- stripping for charge exchange injection, it also set up a first example of using megawatt ultraviolet (UV) laser source in an operational high power proton accelerator facility. This paper reports in detail the design, installation, and commissioning result of a macro-pulsed multi-megawatt UV laser system and laser beam transport line for the laser stripping experiment.

Keywords: Laser; Hydrogen ion; Laser stripping; Charge exchange injection; Spallation Neutron Source

I. Introduction

Advancements in laser technology have dramatically expanded the applications of lasers to high energy physics [1]. Today, lasers have been used in a broad range of particle accelerators from test stands to operational facilities. A number of important applications with different levels of technical readiness have been demonstrated including beam diagnostics [2], photo-injectors [3], Compton scattering-based light sources [4, 5], and laser driven electron acceleration [6, 7]. Recently, a laser assisted hydrogen beam stripping method has been developed at the Spallation Neutron Source (SNS) [8]. The laser stripping technique has the potential to make it possible to stack high-intensity proton beam with no restrictions of beam loss and radiation activation at high beam intensities. Following a successful proof-of-principle demonstration [9] using a Q-switched laser, a more advanced experiment, or a proof-of-practicality experiment was recently proposed by SNS [10] and funded by U.S. Department of Energy (DOE) High Energy Physics Program. The goal of the project is to demonstrate high-efficiency H^- beam stripping at an operational accelerator setting. A typical neutron-production H^- beam at SNS is bunched in a macropulse (burst-mode) structure where each macropulse consists of 30-ps micro-pulses repeating at 402.5 MHz.

Laser stripping imposes a number of challenges on both laser technology and laser operation. First, high efficiency stripping requires lasers with high peak and high average powers in the ultraviolet wavelength regime as well as a complicated macropulse structure, which cannot be obtained using conventional chirped pulse amplification (CPA) technology [11]. Such lasers are not available in the current laser market and demand the development in macropulse amplification technology. Second, high radiation in an operational high power proton accelerator puts significant restrictions on the control/operation of the laser system. Besides, high intensity UV laser beam also introduces risks to accelerator operation, such as the laser induced breakdown on the vacuum windows. In most the above-mentioned applications [2-7], high power lasers have been installed near electron accelerator beamlines where radiation concerns were much insignificant compared to proton accelerators.

In this paper, we describe the design and performance of a macropulse laser system that provides picosecond pulses with multi-MW peak power at 355 nm. The pulses are repeating at 402.5 MHz and are bunched into a burst mode structure with variable macropulse durations and frequencies. We discuss that the general design concept can be adapted to any temporal beam structures in most accelerators. We also describe the implementation of laser transport line (LTL) that delivers UV beam over a 60-meter long complicated beam path with remote control/monitor of laser parameters. The LTL delivered UV beam to the laser stripping location at a 70% efficiency and survived high radiation doses induced by megawatt proton beam accelerator. A laser parameter scalability to the full-cycle laser stripping, i.e., 1 ms macropulse at 60 Hz, is also discussed.

2. Macropulse UV Laser

2.1 Laser parameter requirement

The SNS laser stripping scheme consists of three steps: First, H^- ions are converted to H^0 by stripping off the first electron in a magnetic field; then H^0 atoms are excited from the ground state (n = 1) to an upper level, i.e. n = 3, by a laser; finally the excited states H^{0*} are converted to H^+ by stripping the second electron in a second magnetic field [8]. The bandgap energy between the ground state and the n = 3 state is 12.1 eV which corresponds to a laser wavelength of 102.6 nm. Although some lasers, e.g. excimer lasers, are emitting at the close wavelengths, those lasers are usually operating at continuous-wave (CW) mode with relatively low power. Meanwhile, by taking advantage of the fact that the hydrogen atoms are moving at a relativistic speed, it was shown in [12] that the necessary photon energy to excite H^0 atoms can be greatly reduced. In the case of SNS linear accelerator, the H^- beam reaches a kinetic energy close to 1 GeV (the corresponding H^- ions and H^0 atoms speed are near 87% of the light speed), the wavelength of the laser light in the H^0 atom rest frame can be lowered to around 355 nm if the laser and H^0 beams interact with each other at a certain angle. Such a wavelength can be readily achieved by tripling the frequency of an Nd:YAG laser that is one the most popular high power pulsed light sources.

While the three-step laser stripping concept [12] was proposed several decades ago, a fundamental technical challenge was to deal with the Doppler broadening of the hydrogen absorption linewidth due to the finite momentum spread of the H^{-}/H^{0} beam. Danilov [8] proposed an efficient method to excite all the hydrogen atoms nearly simultaneously by using the Doppler dependence of the hydrogen rest-frame laser frequency. By preparing a diverging laser beam, the interaction angle between the laser and particle beams continuously changes across the hydrogen beam path and accordingly the frequency of the light in the H^{0} atom rest frame decreases as the angle increases. The diverging laser beam introduces an effective frequency ‘‘sweep’’ as the hydrogen beam traverses the laser interaction region, which assures that all atoms with different energies will be excited.

Figure 1(a) shows the calculated stripping efficiency as a function of the laser peak power. Obviously, the stripping efficiency rapidly grows in proportional to the laser power at low power levels while saturates quickly when the laser peak power exceeds 1 MW. The stripping efficiency also depends on the laser beam divergence angle in the interaction plane (assumed in the horizontal plane) and the laser beam size in the perpendicular (vertical) plane, as shown in Fig. 1(b). To obtain stripping efficiency of 90% and above, we need to prepare a UV laser beam with a peak power of 1 MW, typical (horizontal) divergence angle (RMS) around 0.5 mrad and (vertical) beam size around 0.2 mm (RMS).

Temporal structure of the laser beam is another important factor. To minimize the (average) laser power requirement, the laser beam needs to have the same temporal structure as that of the ion beam. The baseline H^{-} beam of the SNS accelerator has a 1 ms pulse length and a repetition rate of 60 Hz. Each macropulse contains micro-pulses bunched by the SNS RFQ at a frequency of 402.5 MHz. For the laser stripping experiment, the pulse width of the micro-pulses is compressed into ~ 27 ps (FWHM).

The goal of the present experiment is to verify the practicality of laser stripping by demonstrating that all individual micro-pulses within a macropulse can be simultaneously stripped at ~ 90% efficiency using a properly designed macropulsed UV laser. The macropulse duration is set at 10 μs in the current experiment. The macropulse duration can be expanded to 1 ms by changing the pump scheme in the proposed amplifier system.

Maintaining the MW peak power over 1 ms is beyond the capability of the present laser technology. On the other hand, by using the power recycling optical cavity, the proposed laser stripping technology is scalable to full-cycle H- beam. A discussion on the scalability will be given in the later part of this paper.

2.2 Macropulse laser system

Figure 2 shows a schematic of the stripping laser system. The laser adopts a master oscillator power amplifier (MOPA) configuration. Primary segments include a fiber seed laser, a macro-pulse generator, multiple-stage Nd:YAG amplifiers, and two harmonic conversion crystals. The seed laser, i.e., the master oscillator, is an actively mode-locked fiber laser pumped by 1480 nm diode lasers. The gain medium is a Ytterbium-doped fiber which supports generation of laser light around 1064 nm. The laser wavelength is controlled via a temperature tuned fiber Bragg grating (FBG) with a tuning factor of 13.3 pm/°C. The temperature of FBG is stabilized at 36.0±0.05°C so that the corresponding wavelength 1064.45 nm maximizes the Nd:YAG amplifier gain. The laser cavity (fiber loop) is also temperature stabilized and the default cavity length corresponds to a round-trip frequency of ~ 4.43 MHz. An electro-optic modulator (EOM) modulates the loss in the laser cavity for the active mode-locking. The phase lock loop circuit in the laser provides a control signal to adjust the cavity length through a piezo-transducer (PZT) so that its round-trip frequency matches a sub-harmonic of the pulse repetition frequency. Fig. 3 shows the measured pulse width as a function of (a) the bias voltage (V_b) of the EOM and (b) phase loop control voltage (V_{ph}) of the seed laser. Stable mode locking is obtained over a quite large range of both parameters. The pulse width shows a sensitive dependence on V_b, which provides an efficient way of pulse width tuning within 55 – 85 ps. The radio-frequency (RF) modulation signal on the EOM is synchronized to an external timing signal at 402.5 MHz with a synchronization accuracy of about 1 ps. The seed laser also has a built-in fiber amplifier which brings the seed laser output power to ~ 200 mW.

The infrared (IR) light pulses from the seed laser have a very low peak power (~ 10 W). To generate MW peak power at 355 nm required by the laser stripping, an amplification factor of ~ 10^6 is needed to directly amplify the seed laser. In this work, the amplification is performed in a burst mode by using solid-state amplifiers. Both the macropulse generation and amplification are conducted in free space. An acousto-optic modulator (AOM) is employed to generate macropulses with adjustable pulse durations, repetition rates, and most importantly arbitrary pulse shapes. The macropulse shaping capability is crucial to combat the effects of gain saturation in the amplifier chain. Since the pulse being amplified is short compared to the lamp pulse, the first part of the pulse envelope sees the highest gain and the gain is depleted as the pulse envelope passes through the amplification rods. To achieve a flat macropulse of the UV light, the macropulse of the seed light is controlled so that the front of the pulse envelope has less energy than the end of the pulse envelope, thus compensating for this gain depletion. The AOM is driven by a voltage controlled RF amplifier at a fixed frequency close to the resonance frequency (41 MHz) of the crystal while the amplitude of the RF signal is controlled by an arbitrary waveform generated on a computer. For the present stripping experiment, the laser is operated at 10-μs macropulse mode. Fig. 4(a) shows a typical macropulse waveform of the UV beam with the peak power of ~ 2 MW. The corresponding control voltage waveform on AOM is shown in Fig. 4(b).

Our custom-built macropulse amplifier has three stages. Each stage consists of a pair of identical Nd:YAG rods with the diameters of 5-, 6-, and 9-mm for amplifier stages 1, 2, and 3, respectively. Both the 5-mm and 6-mm amplifiers are single flash lamp pumped with the first rod pumped from the top and the second rod pumped from the bottom. The 9-mm amplifiers are pumped by two flash lamps from sides. In each amplifier stage, there are two compensation optics between the two rods: a negative lens for thermal lensing compensation and a quartz rotator for thermal birefringence compensation. The amplified IR macropulses are converted to the UV light using a 25 mm long LBO doubler and a 30 mm long LBO tripler. More details of the amplifier can be found in the previous paper [13]. The amplifier was designed to generate 1 MW (peak power) UV pulses bunched in 10-us@10-Hz macropulses. We have implemented a number of improvements in recent years. In particular, maximum gains of the first two amplifier stages have been achieved after proper optics realignment and insertion of an additional isolator between 5- and 6-mm rods. The image relay optics and spatial optical filters have been redesigned to maximize the amplifier output power while maintaining high beam quality. The improvements boosted the maximum peak power of the UV pulses to ~ 3.5 MW, more than three times the design specification.

Fig. 5 shows the IR micro-pulses measured using a high bandwidth photo-detector. A typical micro-pulse waveform is shown in the inset box. The pulse width varies from 55 to 85 ps and the temporal jitter is about 1 ps. Accurate information of the UV pulse width is important in the optimization of pulse energy in the amplification. We have developed a multifunctional optical correlator to measure the pulse width of the UV beam without using any external reference pulse [14]. The correlator measures both auto-correlation between IR pulses and cross-correlation between IR and UV pulses using the same nonlinear optical crystal. We were able to perform a detailed characterization of the UV beam at a variety of amplifier parameters. Fig. 6 shows the measured UV pulse width as a function of the IR pulse width. We also calculated the UV pulse peak power using the measured UV pulse width and UV (average) power. While the UV pulse width is nearly proportional to the IR pulse width, the peak power shows a nonlinear inverse dependence on the pulse width. This is because the harmonic generation efficiency depends on the intensity of the incoming light. As a result, when the seeder pulse width is narrowed from 84 to 54 ps, the UV pulse width changes from 58 ps to 34 ps and the peak power of the UV light increases from 1.2 MW to 3.1 MW.

The UV beam quality is mainly determined by the incoming beam size to the 9-mm amplifier and the entire amplification factor (particularly the setting of the last amplifier). To optimize the beam quality, we set up the 5- and 6-mm amplifiers at their maximum voltages (~ 1.4 kV) while limiting the 9-mm amplifier to relatively low voltages (1.15 – 1.25 kV). Fig. 7(a) shows a near-field profile of the UV beam at ~ 2 MW and Fig. 7(b) shows the far-field profile. The laser beam shows a TEM_{00} Gaussian mode in the far-field and the M^2 factor is measured to be ~ 1.3 in both horizontal and vertical directions. The M^2 factor increases when the peak power exceeds 3 MW.

3. Optical Setup for Stripping Experiment

3.1 Laser transport line

Operating lasers in a proton accelerator facility always faces concerns of radiation induced damage. Although in the previous laser stripping experiment [9] the laser was located in the linac beam dump area, the accelerator was operating with beam powers at the kilowatt level at the time. As the SNS accelerator was ramping up the proton beam power, the residual radiation levels grew rapidly. It was experimentally verified that the laser system (mainly electronics parts) did not survive more than a few hours even in a relatively lower radiation area. Today, SNS is routinely operating at the 1 MW proton beam power level. At this power level, the radiation doses are several orders of magnitude higher than before. In particular, radiation in the Ring injection area reaches tens of kilo-Rads.

To protect the laser from radiation induced damage, we located the macropulse laser system in the Ring Service Building (RSB) and designed a laser transport line (LTL) to deliver the laser beam to the stripping chamber. The RSB is about 10 meters above the beam line and shielded from the accelerator tunnel through a 20-meter thick concrete wall. The only available penetrations between the RSB and tunnel are 6-inch penetration holes which were originally designed as cable chases. A schematic of the LTL is shown in Fig. 8. It consists of three parts: the first part transports the laser beam from the laser table to the entrance of the penetration hole in the RSB, the second part is a 70-ft long cable chase, and the last part relays the laser beam from the exit of the chase to the stripping chamber location in the Ring/HEBT tunnel areas. The entire LTL is enclosed in aluminum tubes and the entrance/exit of the LTL are sealed with 4-inch vacuum viewport windows that are AR-coated at 355 nm. The enclosure is important to eliminate air flow caused by pressure/temperature difference between the RSB and accelerator tunnel.

Although the total length of the LTL is only about 60 meters, due to the existing accelerator beam line, existing electronic and mechanical equipment, the available space for the LTL is extremely limited and the resulting LTL has a very complicated path configuration as shown in Fig. 8. A total of 8 mirrors have to be used to relay the beam in 8 different planes. Table I lists the parameters of each relay mirror. Note that mirrors reflect light at different angles varying from ~ 6° to ~ 50° are used due to the space limitation. All mirrors are 3-inch dielectric mirrors with high-reflection (HR) coating at

355 nm over a wide range of reflection angles (5° – 53°). In addition, most of mirrors are very difficult to access due to radiation/electrical concerns. Therefore, all relay mirror mounts except the first two are equipped with a pair of pico-motor driven actuators for remote control beam steering and a compact analog camera for monitoring of the beam position on the mirror surface. Two examples of the mirror box implementation are shown Fig. 9.

Many conventional laser transport lines employ the image relay approach where beam is focused and collimated between two relay mirrors. This approach turns out to be impractical in the present environment due to the limitation of space for lens mount, lack of control and accessibility. Instead, we chose an approach of propagating a collimated laser beam through the entire LTL without image relay. A series of LTL simulations were carried out on the optical table in the laser lab by using multiple reflections on 8 mirrors to make up a path length close to 60 meters. Using LTL simulations, we compared different telescope settings for beam collimation and studied the transmission efficiency and final beam quality in each case. The optimal transmission performance is obtained when the laser beam is focused close to the final destination. In this case, the laser beam is collimated to have beam diameters of about 10-12 mm ($1/e^2$) along the LTL. The transmission efficiency was estimated to be around 75%. Major beam losses come from the absorption/scattering on the mirror surfaces and loss of high-order modes of the laser beam during the propagation through LTL.

3.2 Stripping experiment optics

The laser stripping experiment is carried out at ~ 20 meters upstream of the SNS ring injection area. As described in the previous section, successful stripping requires a narrow parameter range in laser beam size, divergence angle, and interaction angle between the laser and ion beams. In addition, to avoid possible optical breakdown on the vacuum windows, the minimum beam sizes on the entrance and exit vacuum windows need to be limited. Fig. 10 shows a schematic of the optical setup around the stripping chamber. The telescope consists of a lens pair (f_1 = -100 mm and f_2 = 200 mm) and the spacing between the two lenses is controlled by a stepper motor. The location and spacing of the telescope controls the beam size and divergence angle at the interaction point. Limit switches are implemented at each end of the motor to limit the beam sizes on vacuum windows. The interaction angle is controlled by a steering mirror and a second stepper motor. The entrance and exit windows are located at ~ 40 inches from the focused point of the laser beam by using extension tubes. Laser beam positions are monitored before and after the stripping chamber using two Gigabit Ethernet cameras (Cam1 and Cam2 in Fig. 10). The laser power is monitored also by an Ethernet accessed power meter.

Table II summarizes the major laser parameters measured before the stripping experiment. The laser beam is interacting with a 1 GeV H- beam at 37.5°. At the interaction point, the designed laser beam has a full-width half-maximum (FWHM) beam divergence angle of 1.2 mrad and a FWHM beam size of 0.5 mm. The transmission efficiency was measured to be near 70% which is close to our lab simulations.

3.3 Laser operation and control

Like many other experiments in the accelerator facilities, laser stripping experiments are conducted in the central control room, which requires high level of automation and remote access/manipulation of laser and optical parameters. Table III lists major electronic chassis and computers used in the operation.

The customized macropulse laser amplifier has a sophisticated graphic user interface (GUI) software that allows the users to operate the laser through a computer. Using the accelerator network, one can remotely turn on/off the laser operation, change amplifier settings, switch between different macropulse modes, and monitor the status of amplifiers and optical crystals. The laser power is also remotely controlled using a motor driven rotational stage to control an optical wave plate. There are two levels of temporal synchronization. The micro pulses generated in the seed laser are synchronized to the 402.5 MHz RF timing of the SNS accelerator. The phase difference can be remotely tuned using a computer controlled digital phase shifter with a precision of 0.1 degree (corresponding to ~ 0.7 ps). The laser macropulse is timed to the accelerator according to a beam position monitor near the stripping chamber and its phase is also computer controlled to nanosecond accuracy. Both controls are realized in the extensible display manager (EDM) screen during the lase stripping experiment.

Beam steering in the LTL is implemented using 7 pairs of pico-motor actuators. The Thorlabs open-loop actuators have a very high radiation tolerance and are controlled by a single computer. The same computer also controls two stepper motors in front of the stripping chamber (Fig. 10) to change the laser beam size/divergence angle at the interaction point.

Laser beam positions along the LTL are monitored using Watec analog cameras toward the surface of the mirror. The tiny cameras were chosen since they have reasonably high radiation tolerance, and are easy to install in a limited space. All images are displayed on a monitor next to the laser table to facilitate the alignment. The laser beam positions right before and after the stripping chamber are monitored by two CMOS cameras (Allied Vision GC 750). Both cameras are synchronized to the 10 Hz macropulse timing and the captured images are sent back to the computer through Ethernet network. The images are then analyzed to extract the centroid position which is used to feedback control the piezo-transducer (PZT) mirror mounted right before the LTL on the laser table. The feedback control is very effective in the reduction of slow (<1 Hz) drifts of the laser beam through the LTL [15].

Finally, the laser power after the stripping chamber is measured by a power meter. The measured power determines the actual laser pulse energy in the stripping chamber by taking into account assuming the losses in vacuum windows.

4. Discussions

The present laser stripping experiment has been successfully conducted using a 10-us laser macropulse. A stripping over 10 mini-pulses of the H- beam has been observed with the maximum stripping efficiency close to 99%. Details of experimental results are reported in [10]. Here we briefly discuss the scalability of the present laser stripping scheme to a full-cycle H^- beam, e.g. 1-ms@60-Hz in the case of SNS neutron production operation.

It is clear that the flash lamp pumping scheme in the present laser amplifier is the major limiting factor of the macropulse structure. Typical flash lamps limit the repetition rate to 30 Hz and the pulse duration to ~ 200 μs. The flash lamp limitation can be resolved by using a diode pump scheme. A commercially available 3-stage diode-pumped solid-state laser amplifier can generate multi-millisecond macro pulses [16]. A less obvious limiting factor, however, is the strong dependence of the achievable UV light power on the macropulse duration. In our experiment, we observed that the achievable peak power of the IR pulses rapidly dropped below 1 MW when the macropulse duration was increased to 30 μs. In this case, the peak power of the UV pulses after harmonic conversion is at the 10 kW level, which is two orders of magnitude lower than the required power for laser stripping.

On the other hand, since the cross-section number in the photon-particle interaction in the laser stripping process is extremely small, the power loss of the laser light is negligible. The laser power can be recycled using an optical cavity if the laser stripping is located in the cavity. External optical cavities have been routinely applied to recycle the power from single-frequency lasers or mode-locked lasers which have pico-/femto-second pulses repeating at tens of MHz to GHz. However, for a burst-mode laser, due to a very small duty factor and low repetition rate of the burst, it is impossible to generate an effective error signal within the short duration of the burst. In such a case, the conventional cavity locking technique will fail and a different cavity locking method is demanded. At SNS, we proposed a double-resonance optical cavity (DROC) scheme and developed a robust locking scheme to realize cavity enhancement of burst mode laser pulses. In the prototype experiment, we have shown how a Fabry-Perot based DROC can be simultaneously locked to an infrared (IR) and its third-harmonic ultraviolet picosecond pulses using a frequency shift technique. We have experimentally demonstrated that such a cavity can be applied to enhance burst-mode UV laser pulses with arbitrary burst lengths and repetition rates [17]. The cavity enhancement of UV macropulses was achieved with an enhancement factor of 50. By using diode-pumped solid state amplifier and optical cavity enhancement technology, it is promising to scale the present laser parameters to fulfill the requirement of the full-cycle stripping experiment.

5. Conclusion

We have described the design and commissioning of a macropulse laser system and its transport line for the laser assisted H^- beam stripping experiment conducted at the proton accelerator of the Spallation Neutron Source. The macropulse laser has a MOPA configuration and consists of a mode-locked picosecond pulsed seed laser and a burst-mode Nd:YAG laser amplifier. We have achieved UV pulses with the pulse widths varying between 34 to 54 ps and a maximum peak power over 3.5 MW. A laser transport line is installed to deliver the UV beam to the laser stripping chamber. The LTL has capabilities such as a remote control and monitor of laser parameters including phase delay, beam power, beam size, beam divergence, and interactions angle. A transmission efficiency of 70% has been achieved. A successful stripping with > 90% efficiency has been demonstrated over a 10 μs macropulse by using the developed laser and optical system. We have also discussed the scalability of the present experiment to the parameters required for the full-cycle laser stripping.

Acknowledgements

We acknowledge C. Huang and Y. Takeda for their contributions to the laser and optical system design and diagnostics, J. Diamond and S. Murray III for their technical helps during installation. ORNL is managed by UT-Battelle, LLC, under contract DE-AC05-00OR22725 for the U.S. Department of Energy. This research was supported by the DOE Office of Science, Basic Energy Science, Scientific User Facilities. The work has also been supported by U.S. DOE grant DE-FG02-13ER41967.

References

[1] G.A. Mourou, T. Tajima, and S.V. Bulanov, "Optics in the relativistic regime," Rev. Mod. Phys. 78 (2006) 309.

[2] Y. Honda, N. Sasao, S. Araki, H. Hayano, Y. Higashi, K. Kubo, T. Okugi, T. Taniguchi, N. Terunuma, J. Urakawa, Y. Yamazaki, K. Hirano, M. Nomura, M. Takano, and H. Sakai,, "Measurements of electron beam emittance in the Accelerator Test Facility damping ring operated in multibunch modes," Phys. Rev. ST Accel. Beams 6, (2003) 092802.

[3] I. Will, G. Koss, I. Templin, "The upgraded photocathode laser of the TESLA Test Facility," Nucl. Instr. Meth. A, 541 (2005) 467.

[4] F. Ebina et al, "Laser pulse circulation system for a compact monochromatic hard X-ray source," Nucl. Instr. and Meth. B 241 (2005) 905.

[5] K. Sakaue, M. Washio, S. Araki, M. Fukuda, Y. Higashi, Y. Honda, T. Omori, T. Taniguchi, N. Terunuma, J. Urakawa, and N. Sasao, "Observation of pulsed x-ray trains produced by laser-electron Compton scatterings," Rev. Sci. Instrum. 80 (2009) 123304.

[6] W.P. Leemans, B. Nagler, A. J. Gonsalves, C. Toth, K. Nakamura, C. G. R. Geddes, E. Esarey, C. B. Schroeder, and S. M. Hooker, "GeV electron beams from a centimetre-scale accelerator," Nature Phys. 2 (2006) 696.

[7] J. Faure, C. Rechatin, A. Norlin, A. Lifschitz, Y. Glinec, and V. Malka, "Controlled injection and acceleration of electrons in plasma wakefildes by colliding laser pulses," Nature 444 (2006) 737.

[8] V. Danilov, A. Aleksandrov, S. Assadi, S. Henderson, N. Holtkamp, T. Shea, A. Shishlo, Y. Braiman, Y. Liu, J. Barhen, and T. Zacahria, "Three-step H- charge exchange injection with a narrow-band laser," Phys. Rev. ST Accel. Beams 6 (2003) 053501.

[9] V. Danilov, A. Aleksandrov, S. Assadi, J. Barhen, W. Blokland, Y. Braiman, D. Brown, C. Deibele, W. Grice, S. Henderson, J. Holmes, Y. Liu, A. Shishlo, A. Webster, and I. N. Nesterenko, "Proof-of-principle demonstration of high efficiency laserassisted H- beam conversion to protons," Phys. Rev. ST Accel. Beams 10 (2007) 053501.

[10] S. Cousineau, M. Kay, A. Rakhman, M. Plum, T. Gorlov, Y. Liu, A. Aleksandrov, and A. Shishlo, “First demonstration of laser-assisted H- charge exchange for microseconds duration beams,” submitted for publication.

[11] J. Limpert, F. Roser, D. N. Schimpf, E. Seise, T. Eidam, S. Hädrich, J. Rothhardt, C. J. Misas, and A. Tünnermann, “High repetition rate gigawatt Peak power fiber laser systems: challenges, design, and experiment”, IEEE JSTQE 15 (2009) 159.

[12] I. Yamane, in Summary Report of Session K on H- Stripping, Proceedings of the 20th ICFA Advanced Beam Dynamics Workshop on High Intensity and High Brightness Hadron Beams, Batavia, IL, 2002, AIP Conf. Proc. No. 642 (AIP, New York, 2002).

[13] C. Huang, C. Deibele, and Y. Liu, “Narrow linewidth picosecond UV laser with mega-watt peak power”, Opt. Express 21 (2013) 9123.

[14] A. Rakhman, Y. Wang, F. Garcia, C. Long, C. Huang, Y. Takeda, Y. Liu, “Multifunctional optical correlator for picosecond ultraviolet laser pulse measurement,” Appl. Opt. 53 (2014) 7603.

[15] R. Hardin, Y. Liu, C. Long, A. Aleksandrov, “Active beam position control of high power pulsed laser for laser-based remote diagnostics,” Opt. Express 19 (2011) 2874.

[16] M. N. Slipchenko, J. D. Miller, S. Roy, T. R. Meyer, J. G. Mance, and J. R. Gord, “100 kHz, 100 ms, 400 J burst-mode laser with dual-wavelength diode-pumped amplifiers,” Opt. Lett. 39 (2014) 4735.

[17] A. Rakhman, M. Notcutt, and Y. Liu, “Power enhancement of burst-mode ultraviolet pulses using a doubly resonant optical cavity”, Opt. Lett. 40 (2015) 5562.

Figure captions

Figure 1 Stripping efficiency as a function of (a) laser peak power and (b) laser beam size and divergence angle.

Figure 2 Schematic of macropulse laser system. EOM: electro-optic modulator, AOM: acousto-optic modulator, PZT: piezo-electric transducer, $\lambda/2$: half-wave plate, SPF: single-mode polarization-maintaining fiber, SF: spatial filter, SHG: second-harmonic crystal, THG: third-harmonic crystal.

Figure 3 Seed laser parameter investigation results. (a) Pulse width vs. EOM bias voltage; (b) Pulse width vs. phase control voltage of mode-lock loop. 'U' indicates unstable region.

Figure 4 (a) 10-μs macropulse waveform. (b) Control waveform on AOM.

Figure 5 A typical IR micro pulse waveform detected by a fast photodiode (New Focus 1444). The inset box shows zoom-in pulse shape of a micro pulse.

Figure 6 UV pulse width and peak power vs. IR pulse width measured by the multi-functional optical correlator.

Figure 7 Spatial profiles of UV beam. (a) Near-field and (b) far-field patterns.

Figure 8 Schematic of LTL. (a) LTL in the RSB is linked to (b) LTL in the Ring through a 20-meter long chase indicated by A - A′ in the figure. M1 – M8 are mirrors for relay.

Figure 9 Examples of optics boxes in the laser transport line.

Figure 10 Optical setup around the laser stripping chamber in the accelerator tunnel.

Table I LTL Components

Mirror	Description	Reflection angle	Propagation length (cm)
Mirror #1	LTL Box #1 (RSB) No camera, No picomotor	52°	110
Mirror #2	LTL Box #2 (RSB) No camera, No picomotor	45°	527
Mirror #3	LTL Box #3 (RSB) Pico-motors (2), camera	45°	122
Mirror #4	LTL Box #4 (RSB) Pico-motors (2), camera	35°	2339
Mirror #5	LTL Box #5 (Ring tunnel) Pico-motors (2), camera	5.6°	50
Mirror #6	LTL Box #5 (Ring tunnel) Pico-motors (2), camera	16.9°	311
Mirror #7	LTL Box #6 (Ring tunnel) Pico-motors (2), camera	50.3°	135
Mirror #8	LTL Box #7 (Ring tunnel) Pico-motors (2), camera	45°	2439

Table II Parameters of Stripping Laser

	Required	**Delivered**
Macro-pulse length	10 μs	12 μs
Micro-pulse width	> 30 ps	30 – 50 ps (adjustable)
Peak power	1.5 MW	4.0 MW (at pulse width 35 ps)
LTL transmission efficiency	> 60%	70%
Maximum power at IP	> 1 MW	2 MW @ 33 ps
Horizontal beam divergence (4σ) at IP	1.6 – 2.6 mrad	2.3 – 3.0 mrad
Vertical beam size (4σ) at IP	1.0 – 1.4 mm	1.1 mm
Pointing stability at the IP		±0.10 mm (H) x ±0.11 mm (V)
Maximum peak laser intensity on entrance vacuum window	≤ 100 MW/cm^2	57.9 MW/cm^2 *
Maximum peak laser intensity on exit vacuum window	≤ 100 MW/cm^2	78.6 MW/cm^2 *

*These values were measured on 1 MW peak laser power. At the end of the experiment, the laser power was raised to 2 MW. No laser induced breakdown was observed over 8 hours of influence.

Table III Control electronics

Control Unit	Description
IOC 1	Laser control (remote on/off, amplifier voltage setting)
IOC 2	Laser power control 6 steering mirrors Interaction angle control Laser beam divergence angle control Laser beam size control Horizontal position control
IOC 3	Laser beam pointing stability feedback control using PZT driven mirror
IOC 4	Laser beam position sensing using GigE cameras
IOC 5	Laser power monitor after the stripping chamber

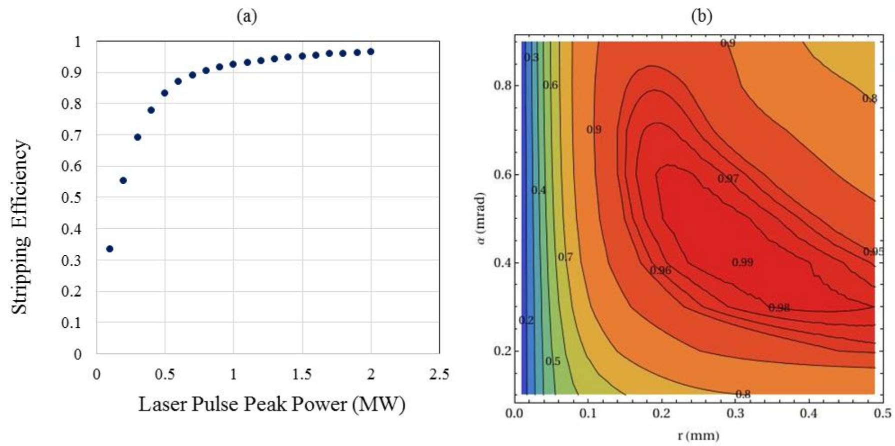

Figure 1

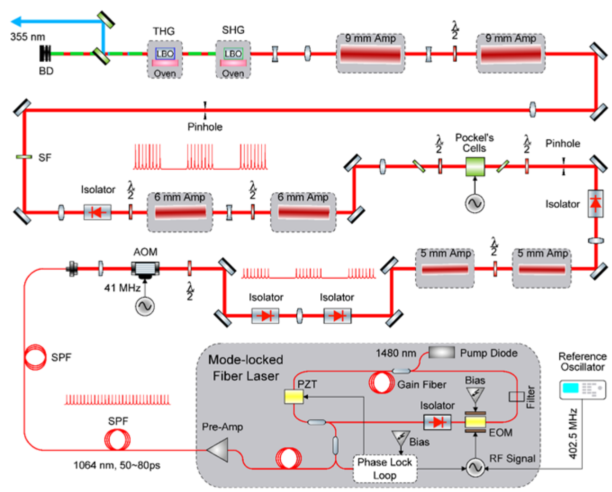

Figure 2

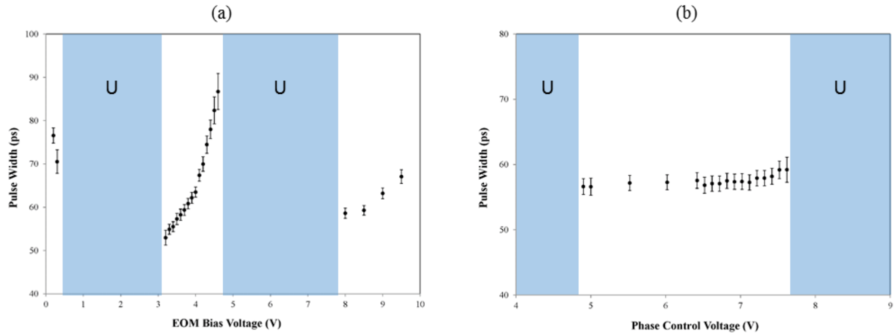

Figure 3

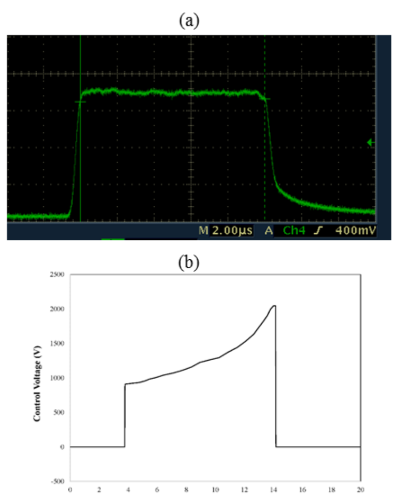

Figure 4

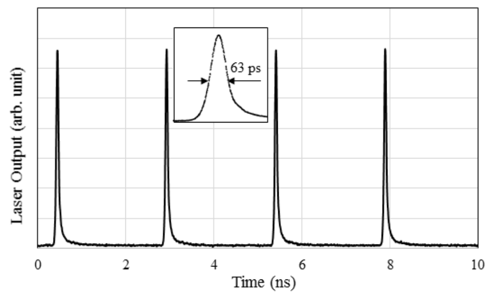

Figure 5

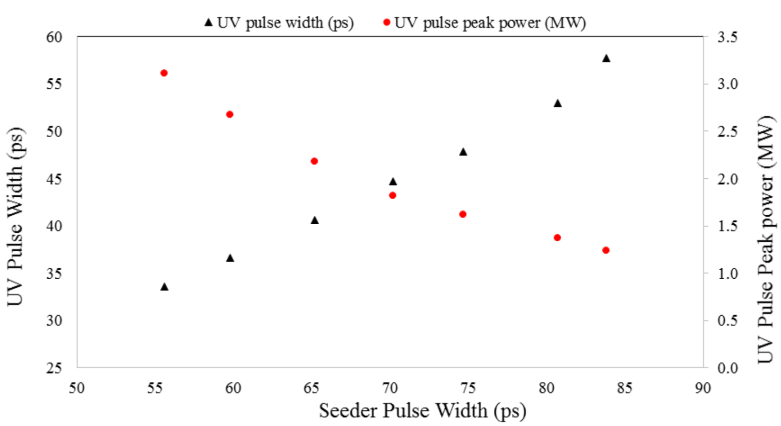

Figure 6

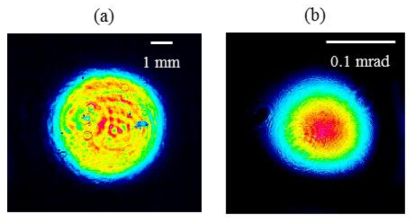

Figure 7

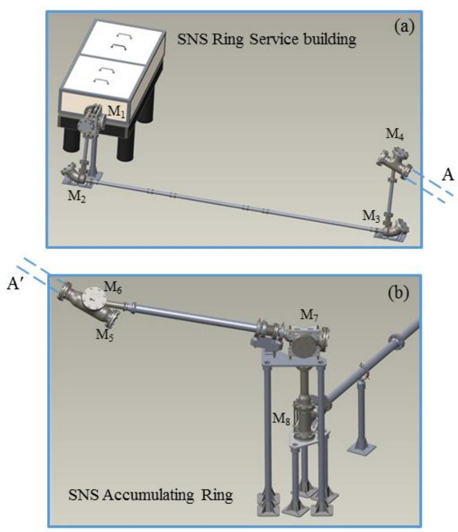

Figure 8

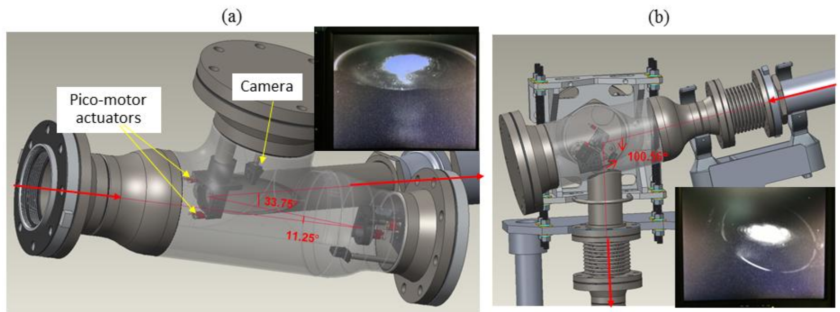

Figure 9

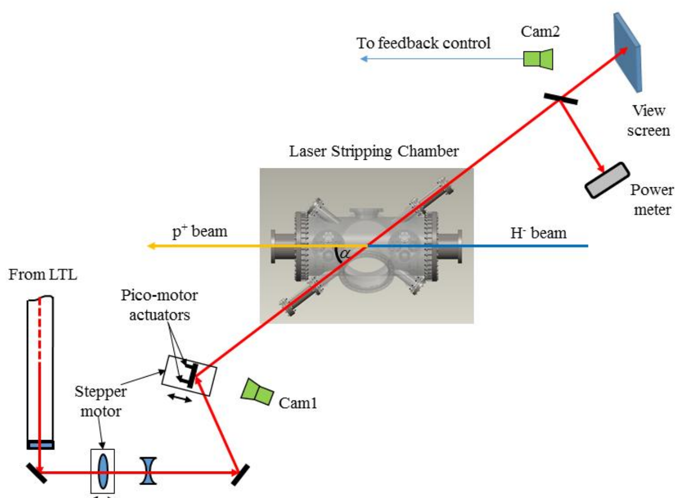

Figure 10

Figure

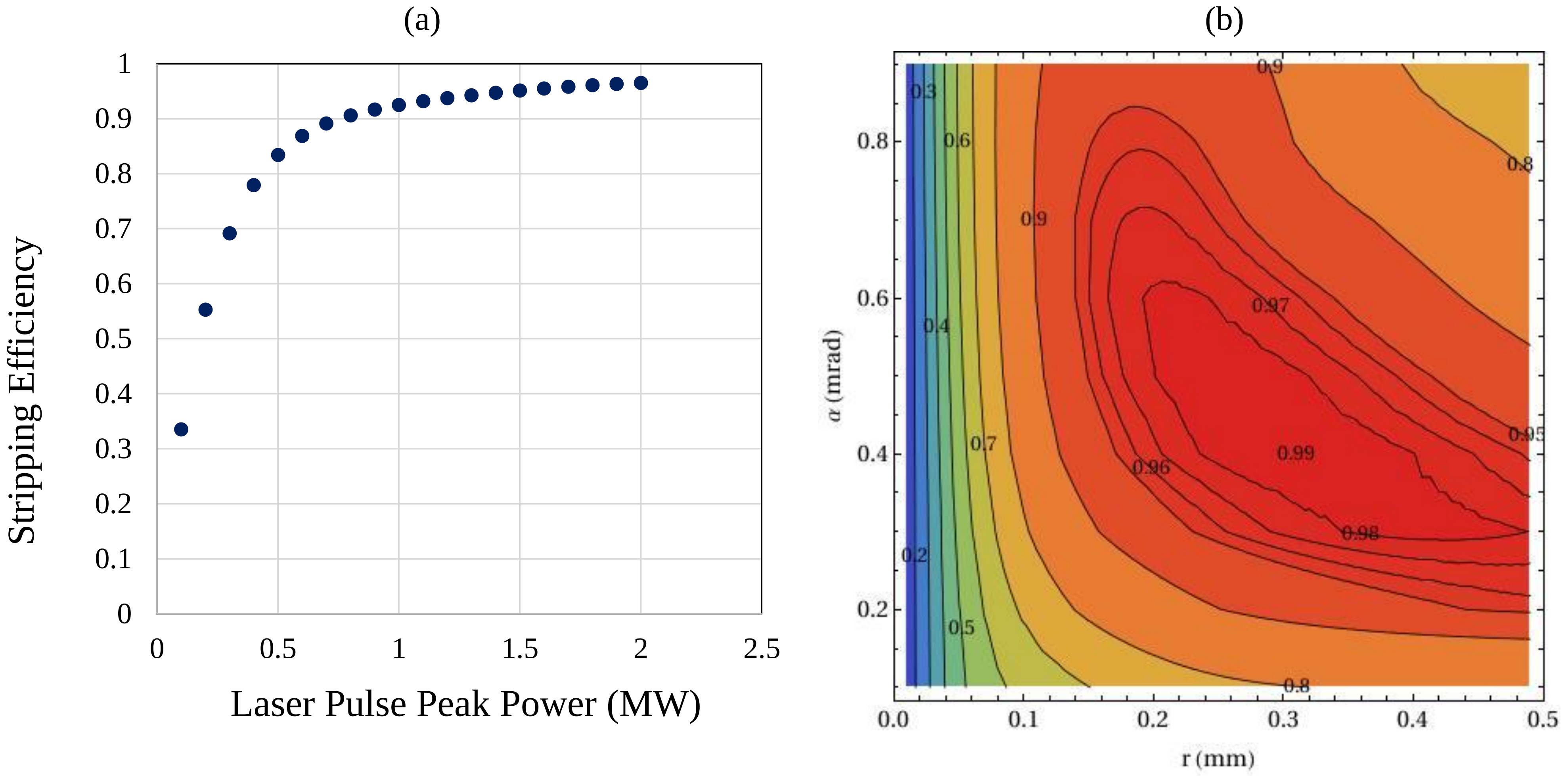

Figure 1

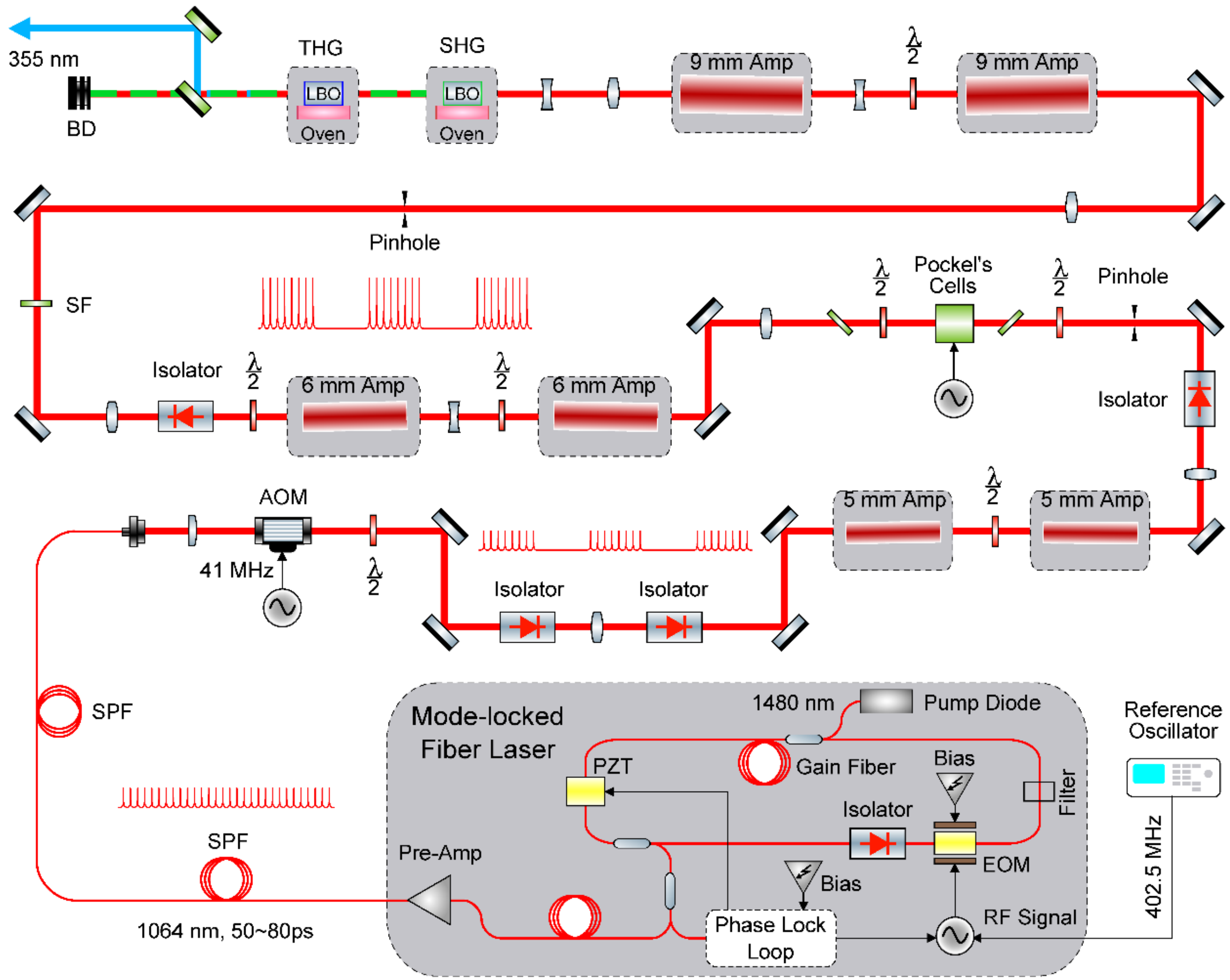
355 nm
BD
THG
LBO
Oven
SHG
LBO
Oven
9 mm Amp
λ/2
9 mm Amp
Pinhole
SF
Isolator
λ/2
6 mm Amp
λ/2
6 mm Amp
λ/2
Pockel's Cells
λ/2
Pinhole
Isolator
AOM
41 MHz
λ/2
Isolator
Isolator
5 mm Amp
λ/2
5 mm Amp
SPF
Mode-locked Fiber Laser
1480 nm
Pump Diode
PZT
Gain Fiber
Bias
Filter
Isolator
EOM
Bias
Pre-Amp
SPF
1064 nm, 50~80ps
Phase Lock Loop
RF Signal
Reference Oscillator
402.5 MHz

Figure 2

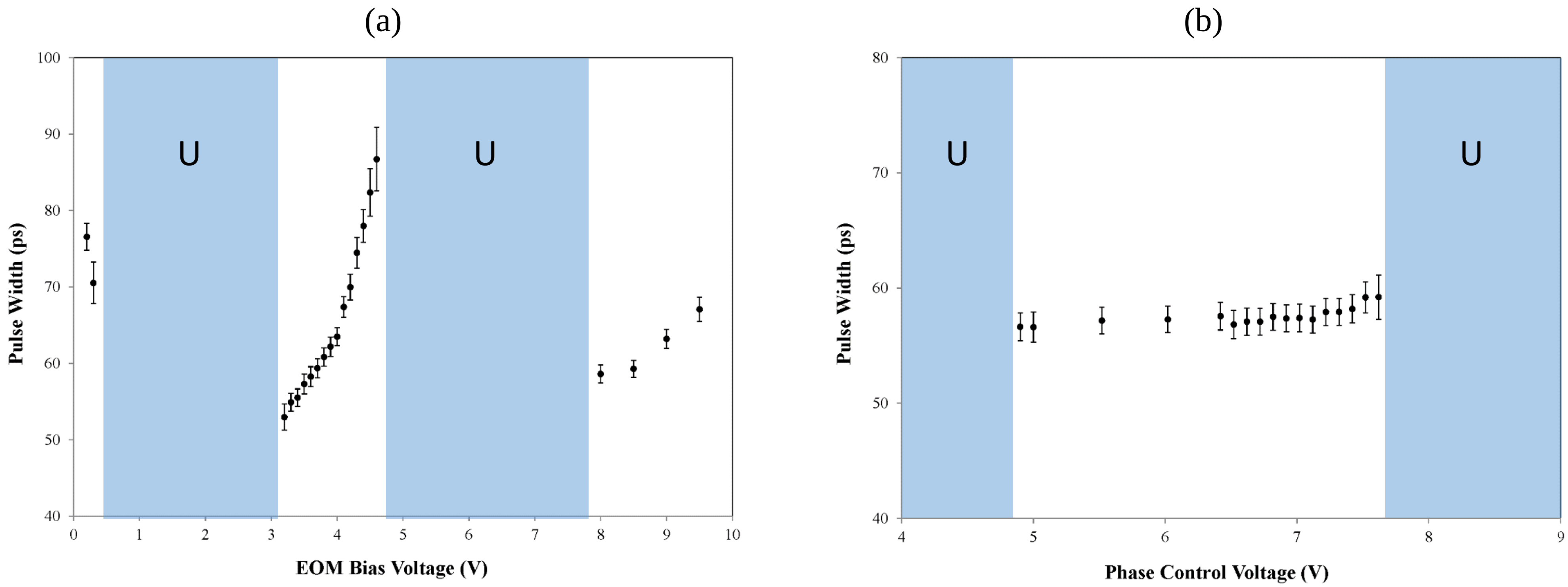

(a)
(b)
U
U
U
U
Pulse Width (ps)
EOM Bias Voltage (V)
Phase Control Voltage (V)
100
90
80
70
60
50
40
0
1
2
3
4
5
6
7
8
9
10

Figure 3

(a)

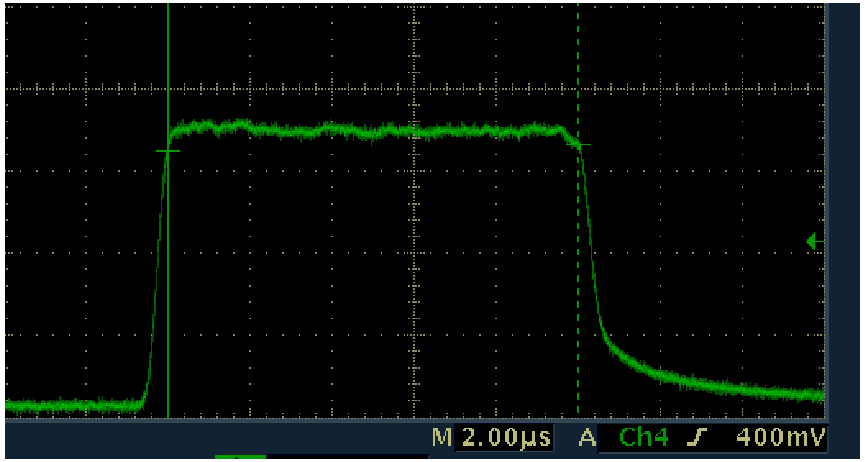
M 2.00µs
A Ch4 400mV

(b)

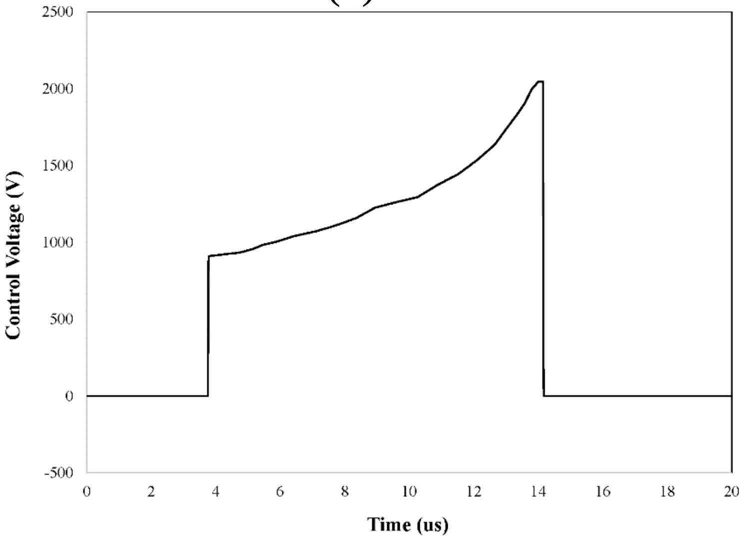
2500
2000
1500
1000
500
0
-500
Control Voltage (V)
0
2
4
6
8
10
12
14
16
18
20
Time (us)

Figure 4

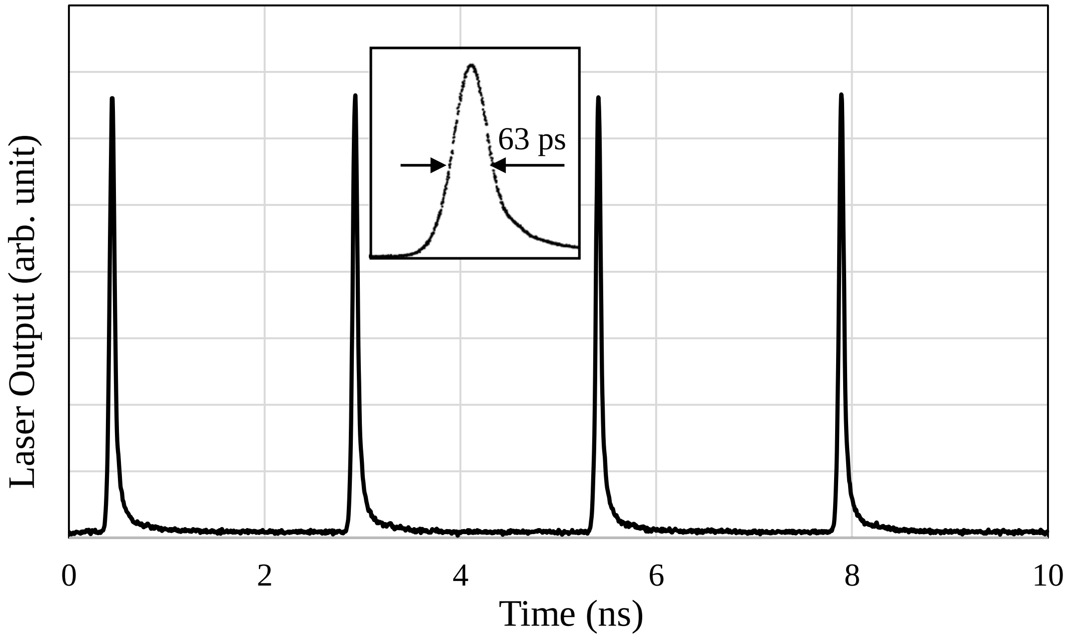

Figure 5

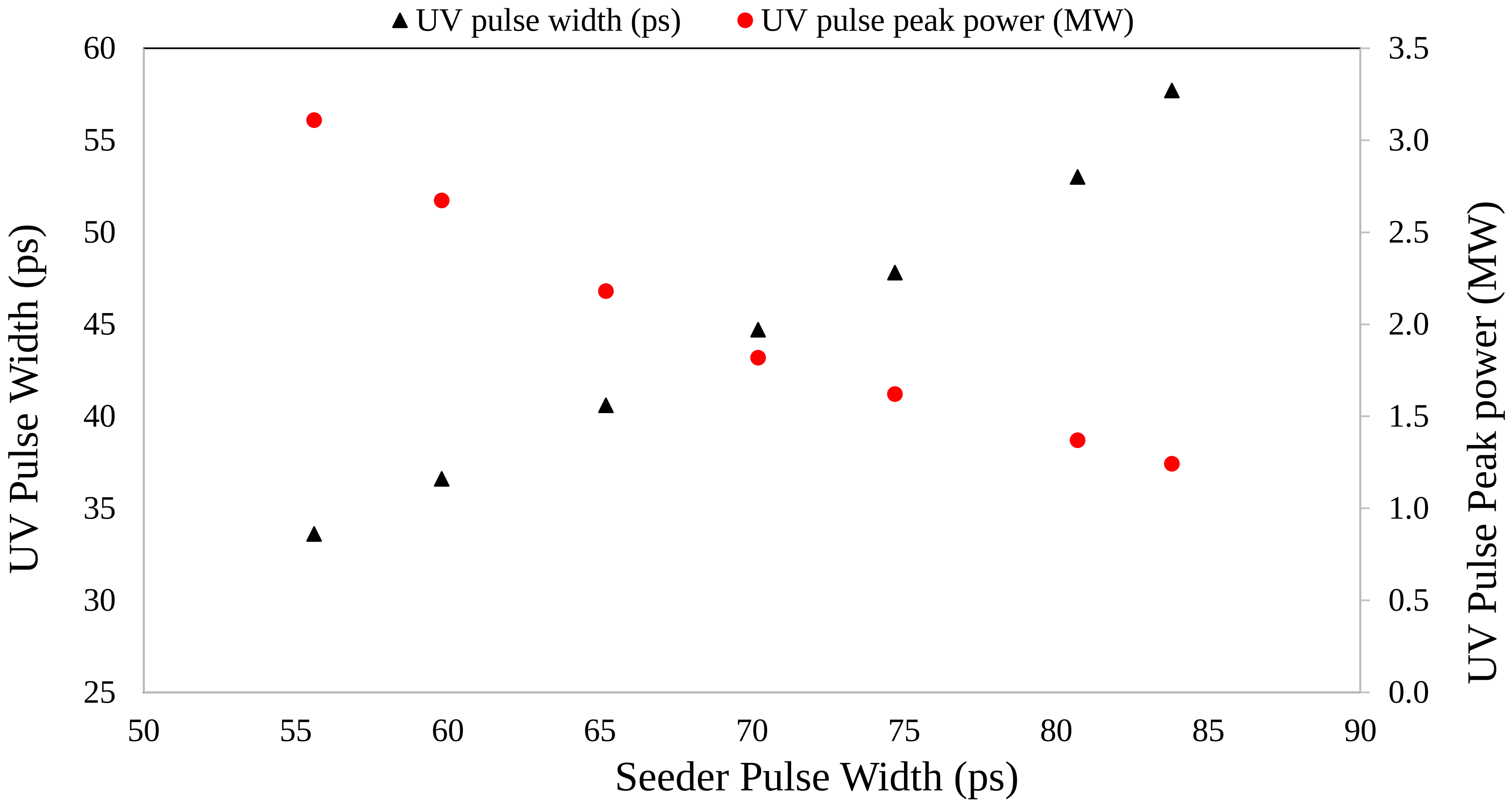

UV pulse width (ps)
UV pulse peak power (MW)
60
55
50
45
40
35
30
25
3.5
3.0
2.5
2.0
1.5
1.0
0.5
0.0
50
55
60
65
70
75
80
85
90
UV Pulse Width (ps)
UV Pulse Peak power (MW)
Seeder Pulse Width (ps)

Figure 6

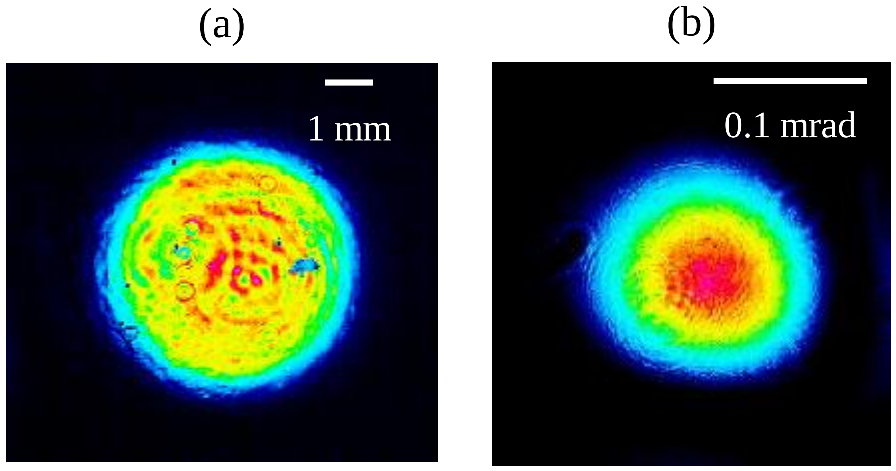

Figure 7

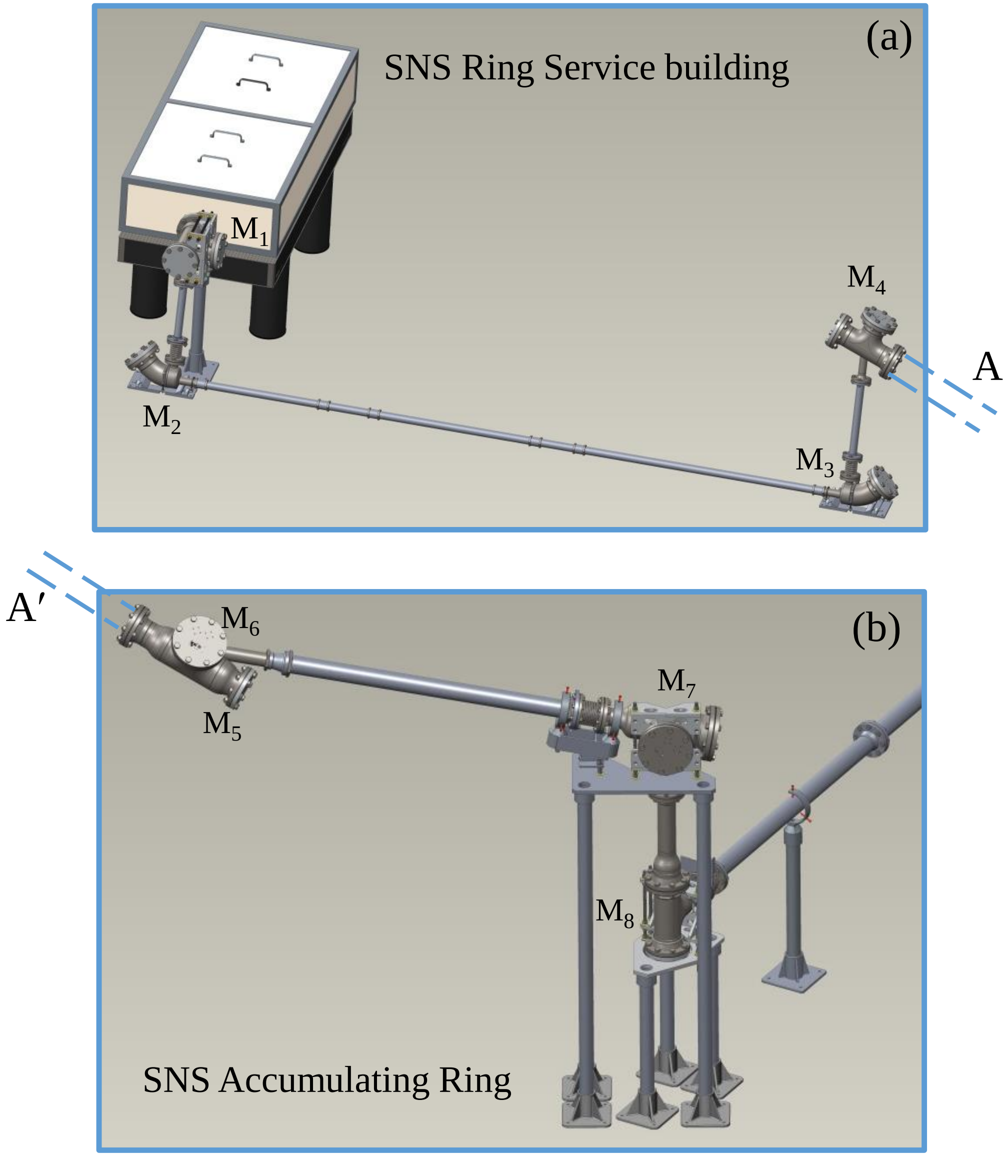

(a)
SNS Ring Service building
M1
M4
A
M2
M3
A′
M6
(b)
M7
M5
M8
SNS Accumulating Ring

Figure 8

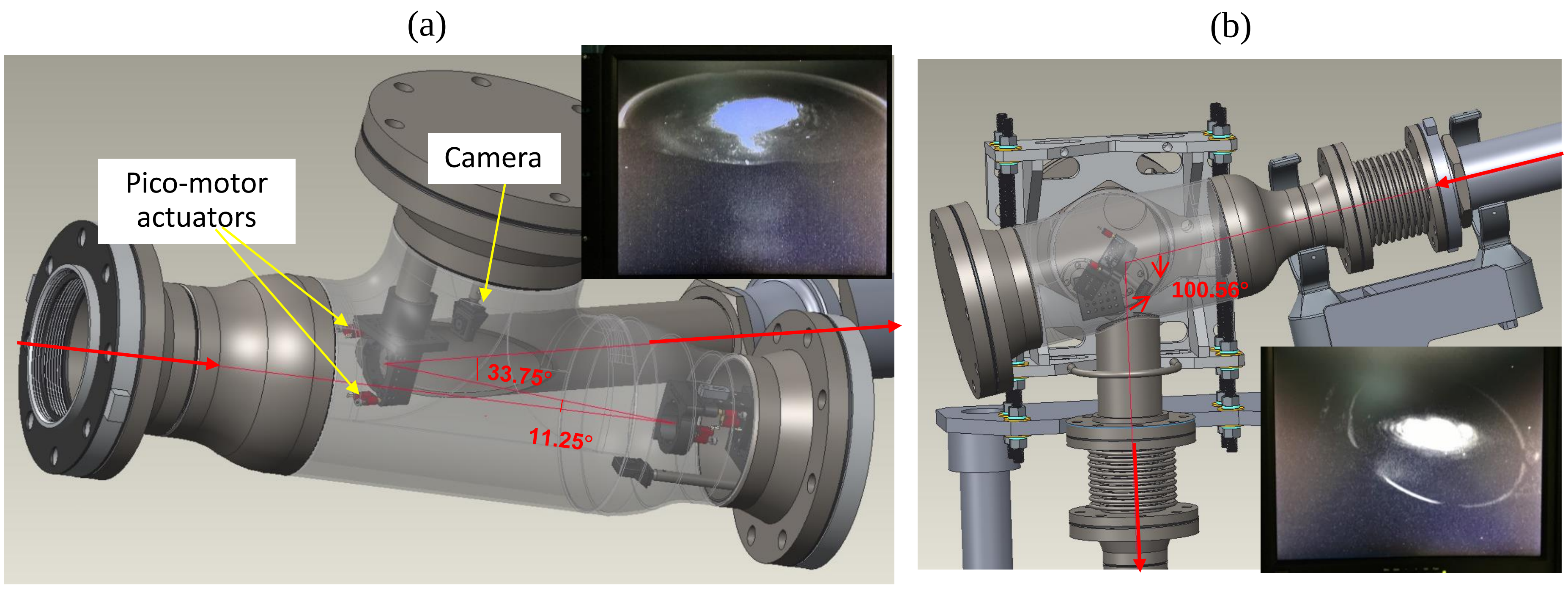

Figure 9

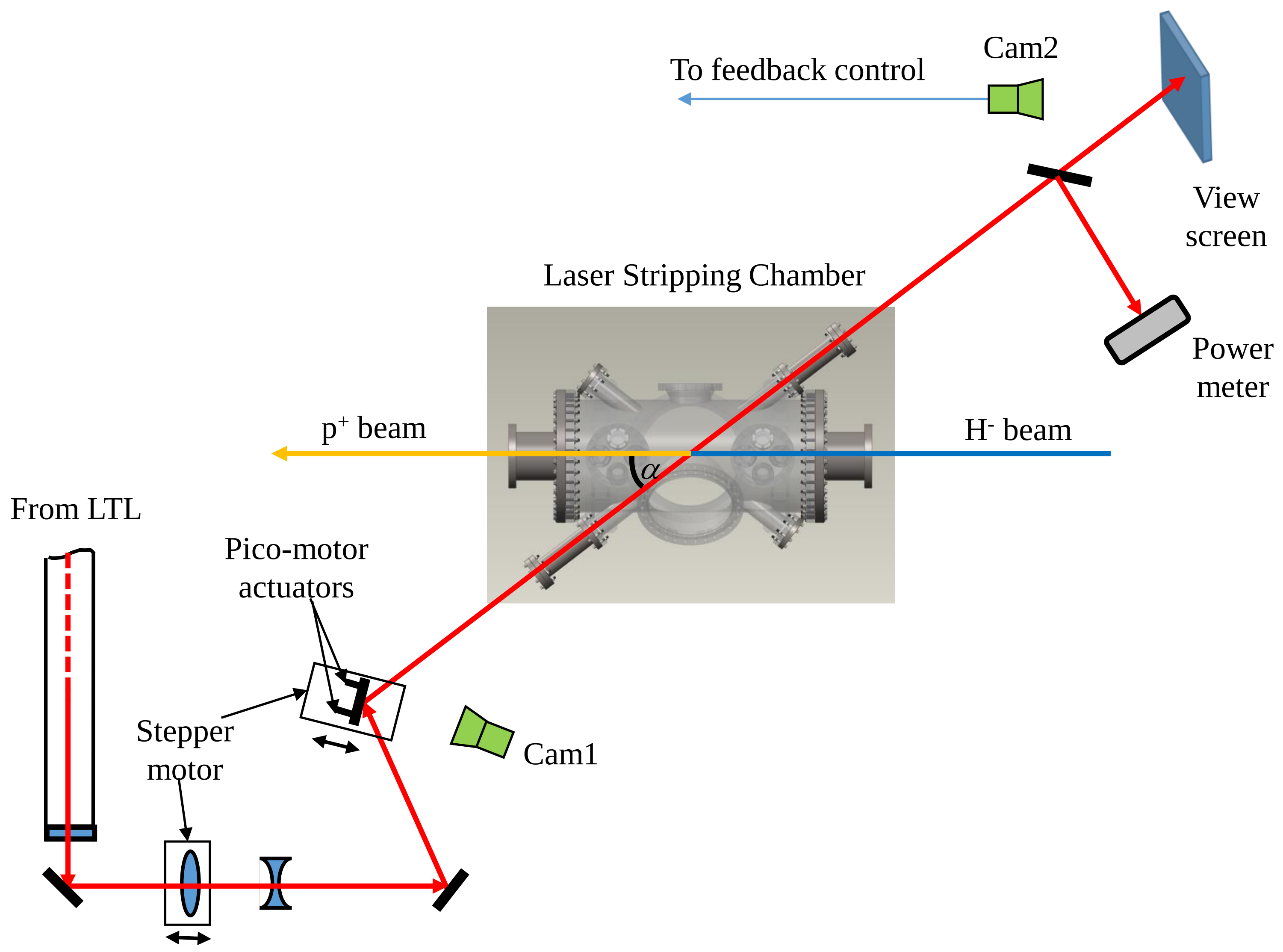

Cam2
To feedback control
View screen
Laser Stripping Chamber
Power meter
p+ beam
H- beam
α
From LTL
Pico-motor actuators
Stepper motor
Cam1

Figure 10